Author(s): Shi, Qixun; Zhou, Xiaohong; Yuan, Wei; Su, Xiaoshi; Neniškis, Algirdas; Wei, Xin; Taujenis, Lukas; Snarskis, Gustautas; Ward, Jas S; Rissanen, Kari; de Mendoza, Javier; Orentas, Edvinas

Title: Selective Formation of S4- and T-Symmetric Supramolecular Tetrahedral Cages and Helicates in Polar Media Assembled via Cooperative Action of Coordination and Hydrogen-Bonds

Year: 2020

Version: Accepted version (Final draft)

Please cite the original version:

Shi, Q., Zhou, X., Yuan, W., Su, X., Neniškis, A., Wei, X., Taujenis, L., Snarskis, G., Ward, J. S., Rissanen, K., de Mendoza, J., & Orentas, E. (2020). Selective Formation of S4- and T-Symmetric Supramolecular Tetrahedral Cages and Helicates in Polar Media Assembled via Cooperative Action of Coordination and Hydrogen-Bonds. Journal of the American Chemical Society, 142(7), 3658-3670. https://doi.org/10.1021/jacs.0c00722

JACS
JOURNAL OF THE AMERICAN CHEMICAL SOCIETY

Article

Selective Formation of S4- and T-Symmetric Supramolecular Tetrahedral Cages and Helicates in Polar Media Assembled via Cooperative Action of Coordination and Hydrogen-Bonds

Qixun Shi, Xiaohong Zhou, Wei Yuan, Xiaoshi Su, Algirdas Neniškis, Xin Wei, Lukas Taujenis, Gustautas Snarskis, Jas S Ward, Kari Rissanen, Javier de Mendoza, and Edvinas Orentas

J. Am. Chem. Soc., **Just Accepted Manuscript** • DOI: 10.1021/jacs.0c00722 • Publication Date (Web): 26 Jan 2020

Just Accepted

is published by the American Chemical Society. 1155 Sixteenth Street N.W., Washington, DC 20036

Selective Formation of S_4- and *T*-Symmetric Supramolecular Tetrahedral Cages and Helicates in Polar Media Assembled *via* Cooperative Action of Coordination and Hydrogen-Bonds

Qixun Shi[†▽]*, Xiaohong Zhou[†], Wei Yuan[†], Xiaoshi Su[†], Algirdas Neniškis[⊥], Xin Wei[†], Lukas Taujenis[¶], Gustautas Snarskis[⊥], Jas S. Ward[#], Kari Rissanen[#], Javier de Mendoza[‡] and Edvinas Orentas[⊥]

[†]Institute of Advanced Synthesis, School of Chemistry and Molecular Engineering, Jiangsu National Synergetic Innovation Center for Advanced Materials, Nanjing Tech University, Nanjing 211816, China

[⊥]Department of Organic Chemistry, Vilnius University, Naugarduko 24, LT-03225 Vilnius, Lithuania

[¶]Thermo Fisher Scientific Baltics, V. A. Graičiūno 8, LT-02241, Vilnius, Lithuania

[#]University of Jyvaskyla, Department of Chemistry, P.O. Box 35, 40014 Jyväskylä, Finland

[‡]Institute of Chemical Research of Catalonia (ICIQ), AV. Països Catalans, 16, 43007 Tarragona, Spain

[▽]State Key Laboratory of Fine Chemicals, Dalian University of Technology, Dalian 116024, China

ABSTRACT: We report on the synthesis and self-assembly study of novel supramolecular monomers encompassing quadruple hydrogen-bonding motifs and metal coordinating 2,2'-bipyridine units. When mixed with metal ions such as Fe^{2+} or Zn^{2+}, the tetrahedron cage complexes are formed in quantitative yields and full diastereoselectivity, even in highly polar acetonitrile or methanol solvents. The symmetry of the complexes obtained has been shown to depend critically on the flexibility of the ligand. Restriction of the rotation of the hydrogen-bonding unit with respect to the metal coordinating site results in a *T*-symmetric cage, whereas by introducing flexibility either through a methylene linker or rotating benzene ring allows the formation of S_4-symmetric cages with self-filled interior. In addition, the possibility to select between tetrahedral cages or helicates, and to control the dimensions of the aggregate, has been demonstrated with three component assembly using external hydrogen-bonding molecular inserts or by varying the radius of the metal ion (Hg^{2+} *vs* Fe^{2+}). Self-sorting studies of individual Fe^{2+} complexes of with ligands of different sizes revealed their inertness toward ligand scrambling.

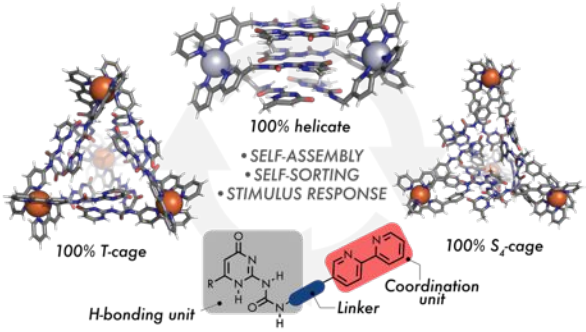

INTRODUCTION

The introduction of the concept of coordination driven self-assembly of simple ligands and metal ions into non-covalent cage structures resulted in the enormous progress of the field of supramolecular chemistry.[1] One-step reliable generation of sophisticated capsule structures from simple precursors enabled researchers to access nanoscopic molecular vessels to experimentally interrogate various molecular phenomena of fundamental importance. Beyond molecular recognition,[2] further developments include enzyme-like modulation of chemical reactivity,[3] stabilization of highly reactive elusive intermediates,[4] selective extraction,[5] sensing[6] and X-ray characterization of analytes by providing ordered solid-state environment for otherwise non-crystalline compounds.[7]

Two families of coordinative molecular cages are currently dominating the field: cavity architectures combining the square geometry of Pd^{2+} with monodentate ligands and metal complexes built upon the octahedral arrangement of bidentate ligands. The latter class of cage complexes enjoys the diversity of molecular topologies (tetrahedron, cube, triple stranded helicate, prism), the use of non-toxic and inexpensive metals (Fe, Zn, Ga *etc*.), and well-established synthetic methods to decorate the metal binding unit (2,2'-bipyridine or related compounds).[8] The selection of a particular shape has been shown to be possible by structural modification of ligands or by a templation effect of the guest.[9] Some of these structures are inherently chiral with asymmetry stemming either from chiral ligands or the metal center itself, and thus provide a platform for enantioselective binding.[10,11] In addition, the reversible nature of coordination bonds enables the building of more sophisticated molecular networks consisting of several ligands and metal ions to explore emerging complexity.[12]

In a classical approach, the coordination cage is built using covalent ligands, synthesized prior to the self-assembly step

(Fig. 1a). To simplify the synthesis and to incorporate dynamicity

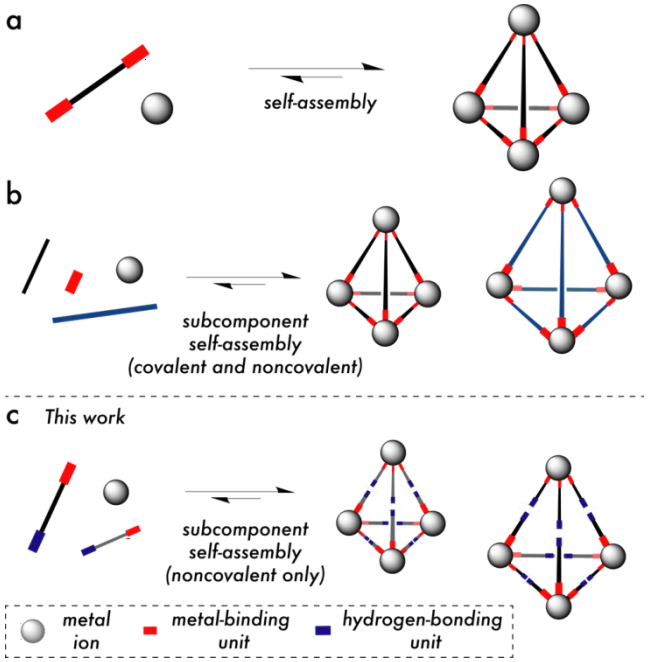

Figure 1. Coordination driven self-assembly exemplified with tetrahedron cages. (a) classical approach with covalent ligands; (b) subcomponent self-assembly combining dynamic covalent and coordinative bonds; (c) newly proposed subcomponent self-assembly employing H-bonded dimers as ligands.

into the system, subcomponent self-assembly, combining both covalent (*e.g.* imine bonds) and coordinative bonds, has been introduced and extensively developed by Nitschke and co-workers as a powerful strategy to construct stimuli responsive dynamic libraries of various supramolecular constructs (Fig. 1b).[13] We speculated that the further extension of subcomponent self-assembly would be possible by incorporating hydrogen-bonding (H-bonding) motifs within the ligand structure, in between the metal coordinating units (Fig. 1c). This would not only allow for an easier synthesis, but also add an orthogonal input channel for external structure modulation. The strong directionality, high sensitivity to polarity of the solvent and temperature, and the possibility for tautomerization[14] define other attractive features of this non-covalent interaction. Despite obvious advantages, the combination of metal and H-bonds as integral elements has not been successfully applied to obtain metal-organic polyhedra and to date, the known examples are limited to planar polygons in non-polar chlorinated solvents only.[15,16] Here we provide the first experimental demonstration of a new class of tetrahedron molecular cages and helicates held together by the cooperative action of coordination and H-bonds in acetonitrile or even methanol and disclose some of their properties.

RESULTS AND DISCUSSION

First generation ligands: design, self-assembly and characterization. Our design of the monomer **1** is outlined in Figure 2a. This compound was synthesized in two steps from reported simple starting materials and features Meijer's ureidopyrimidinone (UPy)[17] as quadruple H-bonding unit together with the metal binding 2,2'-bipyridyl (Bipy) unit, connected through single methylene bridge (for synthesis see the Supporting Information). UPy motif was chosen for its well-known ability to form very stable dimers (up to $K_a = 10^8$ M^{-1} in toluene) whereas Bipy is a ligand of choice for octahedral metal coordination ultimately leading to tetrahedral arrangement of the ligands in the complex. The use of semi-flexible -CH_2- linker to bridge two orthogonal sites was essential for several reasons. First, it provides necessary conformational freedom for the Bipy units to adjust around the metal ion coordination center for optimal binding. Second, by providing limited flexibility and relatively short distances between metal centers, a competing aggregation mode to dinuclear triple-stranded helicate is inhibited due to the steric clash between three bulky UPy_2 dimeric units located close to a helicate axis (Fig. 2b).

Considering the stereochemical outcome of the M_4L_{12} assembly process, there are three possible diastereomers for the most commonly occurring *all*-fac coordination mode, belonging to the symmetry point groups T, C_3 or S_4. It is very common that either the pure homochiral (racemic mixture of ΔΔΔΔ and ΛΛΛΛ enantiomers) T-isomer or the mixture of all stereoisomers is obtained. However, it has also been shown that the extent of stereochemical communication between metal centers, and thus the ratio of the isomers, is sensitive to the structure of the ligand.[18] With regard to isomerism, in the bifunctional ligand **1** containing UPy moieties, the tetrahedral assemblies might also form *via* dimerization of self-complementary enolic forms of the UPy unit (Fig. 2b). In this case, the isocytosine side chains will change the position with respect to the edges of the so-formed tetrahedron moving from equatorial in keto-dimer to parallel arrangement in enol-dimer. Although the formation of tetrahedral complexes is possible for both tautomers, larger substituents might favor the formation of the enol-cage as side chains experience less steric interaction in this aggregation mode.

In order to prove the concept and probe the impact of the bulkiness of the UPy_2 dimer on the diastereoselectivity of the cage formation, five different substituents R (H, Me, *n*-Bu, *n*-$C_{11}H_{23}$ and 3,4,5-tridodedecyloxyphenyl) were attached to UPy. The complex formation was then accomplished by simply mixing the monomer **1** and $Fe(OTf)_2$ in a 3:1 ratio in d_3-acetonitrile under ambient atmosphere. The formation of the complexes was evident from the appearance of deep red color and the dissolution of otherwise insoluble ligands. To our delight, in case of monomers **1a** (R = H) and **1b** (R = Me), well-defined ^{1}H NMR spectra were obtained consisting of three sets of resonances of equal integral intensities (Fig. 2c). Based on symmetry arguments, it was assigned to the exclusive formation of the S_4-symmetric M_4L_{12} cage.[19] The downfield chemical shifts of the N-H resonances clearly indicate the establishment of quadruple H-bonds. In addition, DOSY NMR analysis was also in agreement with the presence of a single species. Namely, all resonances in the spectrum correlated to a single diffusion coefficient of $D = 5.00 \times 10^{-10}$ m^{2}s^{-1} (**1a**) and $D = 4.83 \times 10^{-10}$ m^{2}s^{-1} (**1b**), which translate into hydrodynamic radii $R_H = 1.10$ nm and $R_H = 1.14$ nm, respectively. The values obtained agree well with the radius of circumscribed sphere calculated for the molecular model of the S_4-Fe_4(**1b**)$_{12}$ tetrahedron (see Fig. S91). Electrospray ionization mass spectrometry (ESI-MS) also confirmed the formation of tetrahedron assemblies (Fig. 2e and Fig. S94-95, S97).

In order to fully characterize the supramolecular aggregates in solution, detailed NMR studies were undertaken. As shown in Figure 2d, the keto and enol tautomeric forms and their dimers can be distinguished based on the expected specific through-

bond and through-space interaction map as outlined in Figure 2d using dimer $(\mathbf{1b})_2$ as an example. Based on the ROESY correlation observed between the protons at 12.58 ppm, 12.56 ppm and 12.37 ppm (labeled in blue in Fig. 2c) with isocytosine methyl group protons **d**, the former was assigned as N-H protons **a,** and thus confirm the involvement of the keto form in quadruple H-bonding. Likewise, the COSY and ROESY cross-peaks of N-H proton resonances at 10.52 ppm, 10.32 ppm and 10.30 ppm (labeled in green in Fig. 2c) with CH_2 resonance **e** allows unambiguous assignment of these protons as **c**. Moreover, characteristic long-range W-type COSY coupling of N-H protons **a** to C(sp^2)-H proton **f** of the isocytosine ring as well as ROESY interaction between protons **b** and **c** fully corroborates the above assignments (Fig. 2d). The same spectral features are also observed for complexes obtained using ligands **1a, 1c** and **1d** or by exchanging Fe^{2+} to Zn^{2+} (Fig. 2c, bottom, see the Supporting Information).

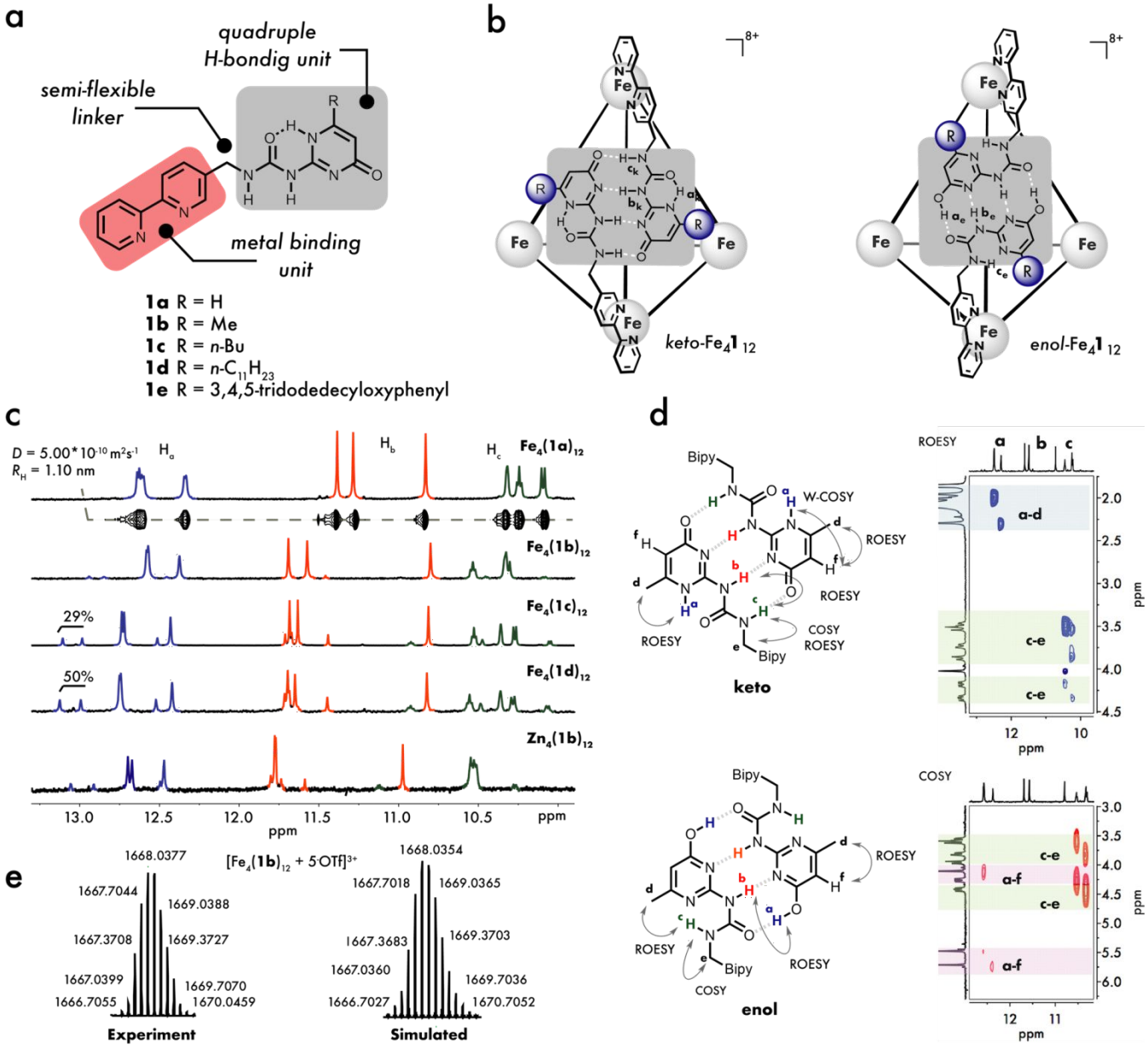

Figure 2. (a) Design of the first-generation ligand **1**; (b) Two possible $Fe_4\mathbf{1}_{12}$ tetrahedral complexes based on keto and enol tautomers of UPy; (c) ^{1}H NMR spectra of S_4-symmetric tetrahedral complexes with DOSY trace. The resonances of the minor species and their quantities are indicated; (d) Characteristic through-bond and through-space interaction maps for keto and enol UPy dimers for ligand **1b** (left) together with obtained ROESY and COSY spectra (right); (e) An example of experimental and simulated ESI-HRMS isotopic patterns for S_4-$Fe_4(\mathbf{1b})_{12}$.

Interestingly, increasing the size of UPy substituents in **1c** and **1d** gives rise to an additional three sets of resonances of lower intensities (Fig. 2c). Initially thought to belong to the enolic form of the UPy, these minor resonances were shown to be part of the keto tautomer, giving the same characteristic ^{1}H-^{1}H cross-peaks as described above. Careful inspection of the ROESY spectra, however, revealed some subtle differences in the surroundings of proton **c** (see Fig. S35, S38). Most likely, the minor species observed are due to different arrangement of the

UPy dimers caused by bulkier butyl and undecyl chains in **1c** and **1d**, respectively, resulting in slowly equilibrating conformers. The DOSY spectra indicate similar hydrodynamic radii of the minor and major species (Fig. S36, S39). Increasing the size of the isocytosine substituent even further as in monomer **1e**, eventually prevents the formation of a tetrahedron cage leading to a broad undefined ^{1}H NMR spectrum, and only ions of smaller complexes $Fe_n(\mathbf{1e})_m$ are detected in the ESI-MS spectrum (Fig. S96). Dilution of the solution of S_4-$Fe_4(\mathbf{1b})_{12}$ in acetonitrile with diethyl ether provided a red precipitate. The recorded ^{1}H NMR spectrum of the freshly dissolved crystals showed only the major conformer, which gradually returned to an equilibrium mixture.

The ^{1}H NMR spectra of the tetrahedral complexes S_4-$Fe_4(\mathbf{1a\text{-}c})_{12}$ show that the chemical shifts of some proton resonances greatly differ from those of the other two of the same type, indicating their unique chemical environment. For instance, the resonances of vinyl proton **f** at 4.01 ppm in S_4-$Fe_4(\mathbf{1b})_{12}$ is shifted upfield ($\Delta\delta$ = 1.40 ppm), whereas resonance **c** at 10.52 ppm is shifted downfield compared to the other two **c** resonances (Fig. 2c, Fig. 3c and Fig. S20, S25, S34, S37). The molecular models for S_4-$Fe_4(\mathbf{1b})_{12}$ obtained using semi-empirical PM7R8 method show a highly deformed tetrahedron with negligible internal cavity (Fig. 3a-b). Compared to the structure of the hypothetical T-$Fe_4(\mathbf{1b})_{12}$ complex, the former features a geometry where all UPy_2 dimers within the ligand $(\mathbf{1b})_2$ are forced to move into the cavity as a result of the connecting CH_2 groups, which dictates the ligands' bent shape. Although the

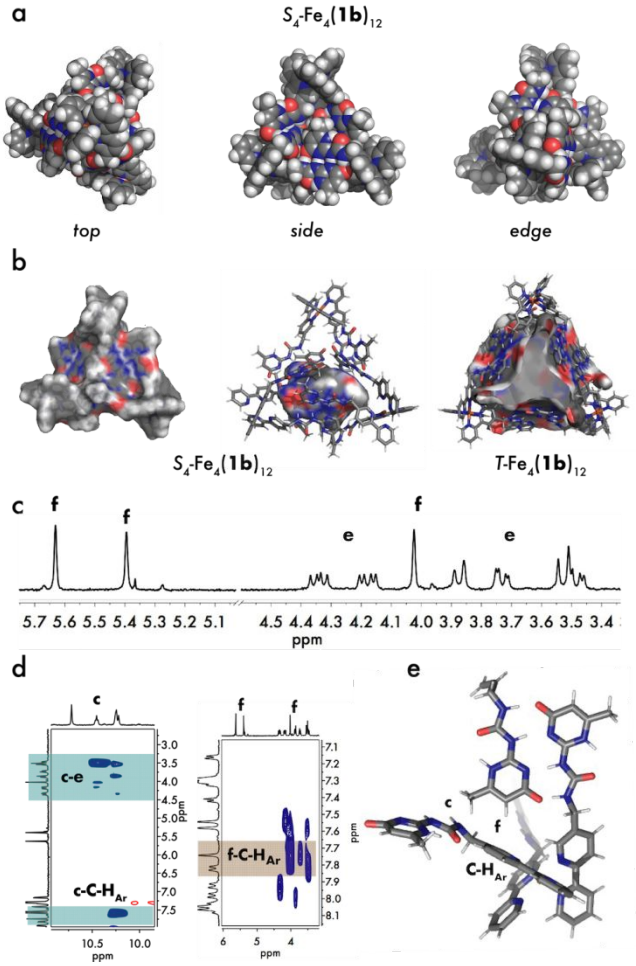

Figure 3. (a) Molecular model of S_4-$Fe_4(\mathbf{1b})_{12}$; (b) Surface of S_4-$Fe_4(\mathbf{1b})_{12}$ (left) and cavity (middle) compared with cavity of hypothetical T-$Fe_4(\mathbf{1b})_{12}$ (right); (c) Extended section of ^{1}H NMR spectrum (400 MHz, CD_3CN) of S_4-$Fe_4(\mathbf{1b})_{12}$; (d) Selected parts of ROESY spectrum of S_4-$Fe_4(\mathbf{1b})_{12}$; (e) Closeup view of molecular model showing spatial arrangement of protons **c**, **f** and C-H_{Ar}.

computationally obtained model is perhaps not fully accurate, it provides some important clues regarding the data obtained from the ^{1}H and ROESY NMR spectra. The most downfield proton of the **c** subset is unique as it gives no cross-peak with the Bipy C-H_{Ar} protons (Fig. 2d and 3d) indicating that it assumes a conformation with rather large distance between these protons. Moreover, in contrast to the downfield protons **f**, the most upfield proton **f** at 4.01 ppm gives a cross-peak with C-H_{Ar}, indicating their proximity. As seen from the molecular model, proton **f** of the isocytosine ring is located inside the tetrahedron and nearby the Bipy ring, experiencing significant shielding (Fig 3c-e). In addition, a weak cross-peak between protons **c** and **f** is also in accord with the calculated structure (Fig. S26).

The small cavity within the S_4-symmetric cage suggests that the formation of the cage complex most likely requires no anion templation. The exchange of a triflate counterion with BF_4^-, BPh_4^-, SbF_6^-, Br^- or $C_{12}H_{25}OSO_3^-$ did not affect the symmetry and resulted in no change of the ^{1}H NMR spectrum (Fig. S29-S33).

Second generation ligands: effect of the linker and conformational rigidity. In order to gain more insight into the importance of the flexibility and length of the ligand on the symmetry of the complexes, two new rigid monomers **2** and **3**, lacking methylene linkers, were synthesized. In monomer **2**, the Bipy unit is connected to UPy directly through the urea functionality, whereas monomer **3** features an additional benzene ring spacer (Fig. 4a-b). The ^{1}H NMR spectra of complexes obtained using $Fe(OTf)_2$ and $Zn(OTf)_2$ as metal ion

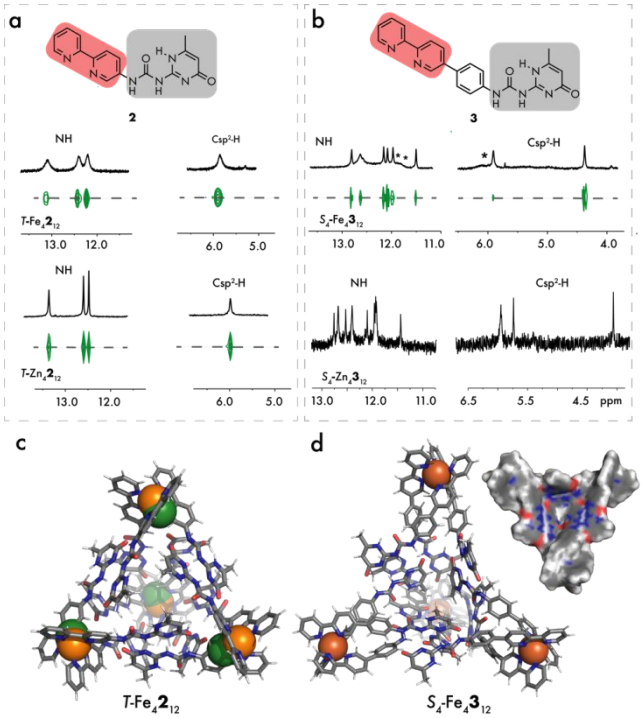

sources in

Figure 4. (a-b) Chemical structures of ligands **2**-**3** and selected parts of ^{1}H NMR and DOSY spectra of *T*-Fe$_4$**2**$_{12}$, *T*-Zn$_4$**2**$_{12}$, *S*$_4$-Fe$_4$**3**$_{12}$ and *S*$_4$-Zn$_4$**3**$_{12}$. Broad resonances are labelled with *; (c) Molecular model of *T*-Fe$_4$**2**$_{12}$. Experimentally determined and calculated Fe^{2+} ions are labelled in green and orange, respectively; (d) Molecular model of *S*$_4$-Fe$_4$**3**$_{12}$. Insert shows the surface of the cage.

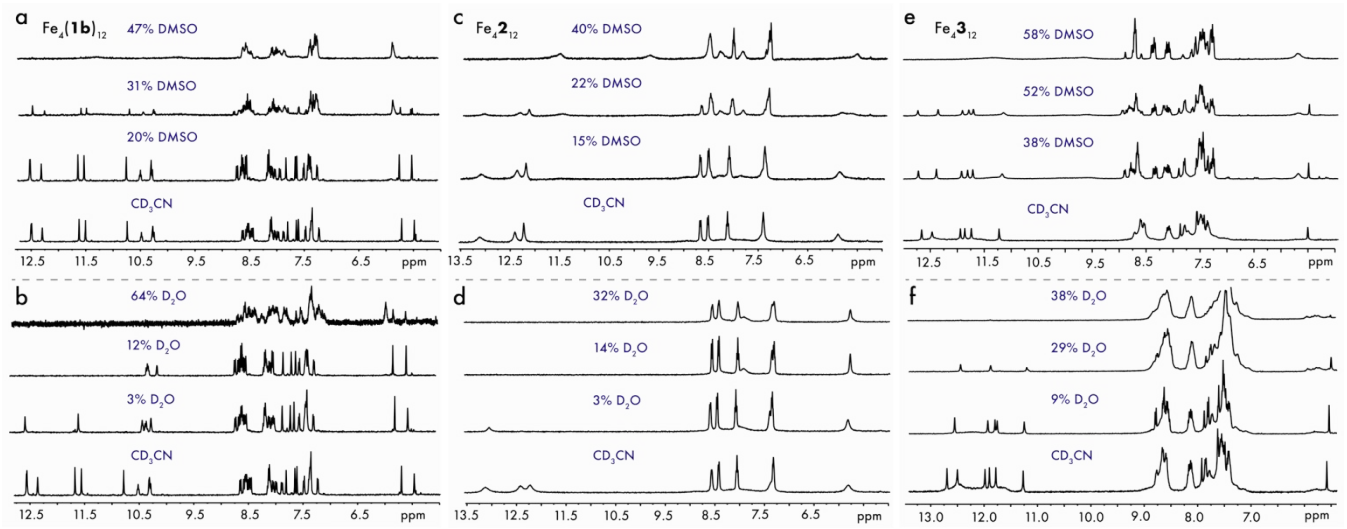

Figure 5. Selected ^{1}H NMR spectra of titration experiments of *S*$_4$-Fe$_4$(**1b**)$_{12}$ (a-b), *T*-Fe$_4$**2**$_{12}$ (c-d) and *S*$_4$-Fe$_4$**3**$_{12}$ (e-f) CD_3CN solution with d_6-DMSO (top) and D_2O (bottom). The content of the competing solvent was calculated as [V(solvent)/(V(solvent)+V(CD_3CN))]*100%, V = volume.

(three sets of resonances) cage for monomer **3**. The DOSY spectra confirm the formation of a single species in all cases. The molecular ions corresponding to a tetrahedral (Fe-Zn)$_4$(**2**-**3**)$_{12}$ cage were observed in the ESI-MS spectra and agree well with simulated isotopic patterns. In the case of Fe$_4$**3**$_{12}$, a trace amount of cubic Fe$_8$**3**$_{24}$ was also detected by ESI-MS (Fig. S99). Some of the resonances in the N-H region and one of the resonances in the C(sp^2)-H region in the spectrum of *S*$_4$-Fe$_4$**3**$_{12}$ were not fully resolved due to broadening, however, they were clearly visible in the spectrum of *S*$_4$-Zn$_4$**3**$_{12}$. Vapor diffusion of chloroform into an acetonitrile solution of *T*-Fe$_4$**2**$_{12}$ allowed the isolation of single crystals. However, the crystals were found to be very weakly diffracting, even with extremely prolonged exposure times using Cu radiation. This is routinely observed for supramolecular species, especially when they are comprised of predominantly light atoms, as is the case for the cages described herein. As expected for supramolecular complexes with a high void volume, the data collected for this structure suffered from rapid fall-off of reflection intensity at high diffraction angles, and this had a negative impact on the quality of the high angle reflections collected, with some not being observed. Fortunately, the positions of the heaviest atoms present (Fe) could be located with high certainty. The perfectly tetrahedral arrangement of four Fe^{2+} ions, separated by 16.1 Å, was found, supporting the formation of the *T*-symmetric cage Fe$_4$**2**$_{12}$. Overlay of experimentally determined coordinates of Fe^{2+} ions with the computationally obtained structure resulted in good agreement (<0.6 Å error) (Fig. 4c). The X-ray quality crystals of *S*$_4$-Fe$_4$**3**$_{12}$ could not be obtained and the molecular model of the cage is shown in Figure 4d. The hydrodynamic radii for *T*-Fe$_4$**2**$_{12}$ and *S*$_4$-Fe$_4$**3**$_{12}$ extracted from DOSY spectra also agree well with the ones obtained from the above models (Fig. S91).

CD_3CN indicate the quantitative formation of a *T*-symmetric (one set of resonances) cage for monomer **2** and a *S*$_4$-symmetric

When taken together, it can be noted that the supramolecular ligands **1**-**3** show a preference for *S*$_4$-symmetry wherever the flexibility of the ligand allows it. Owing to the many available conformations of **1**$_2$ and distances between Bipy units due to unrestricted rotation around the -CH_2- linker, a deformed *S*$_4$-symmetric cage is formed easily and is stabilized by multiple non-covalent inter-ligand interactions (internal solvation) inside the cavity. Ligand **2**$_2$ is completely flat because of the conjugation of the urea nitrogen lone pair with the Bipy aromatic system. Although a *syn* ligand geometry is still possible, the capability of the system to adjust for optimum packing is limited, and therefore the most symmetric *T*-geometry is adopted with all UPy_2 dimers located at the maximum distance from each other, tangential to the tetrahedron surface. Finally, in the case of ligand **3**$_2$, the Bipy and urea moieties are twisted almost perpendicular with respect to the benzene ring linker for the *anti*-configuration, whereas such a twist angle for the *syn*-configuration is much smaller.[18] In contrast to the fully covalent rigid ligands reported in the literature, the distance between Bipy units, and thus between the metal ions, can also be modulated by distorting the quadruple H-bonding motifs from coplanarity. As demonstrated previously with other supramolecular systems, quadruple H-bonds can tolerate bending up to ca. 20° and 10° with respect to the center or the plane of the H-bonding interface, repectively.[14e,f] The molecular model shows that within the shortest edge comprising *anti*-conformer of ligand **3**$_2$, the UPy units are unidirectionally twisted along the line of quadruple H-bonding interface resulting in a distorted V-shaped geometry and reduced distance between metal centres. The preferential formation of the *S*$_4$-symmetric cage is most likely governed by partial accommodation of the UPy_2 dimers inside the cavity of the cage owing to a significantly larger cavity size as compared to *T*-Fe$_4$**2**$_{12}$. Indeed, the void volume of *S*$_4$-Fe$_4$**3**$_{12}$ is not

significant and the assembly resembles more a molecular bowl with open cavity rather than a cage (Fig. 4d).

Stability studies: **effect of solvent polarity and competing agents**. The quantitative formation of tetrahedron cages in acetonitrile indicates the high stability of quadruple H-bonds even in such polar solvents. To further probe the strength of H-bonding in these assemblies, we conducted more detailed

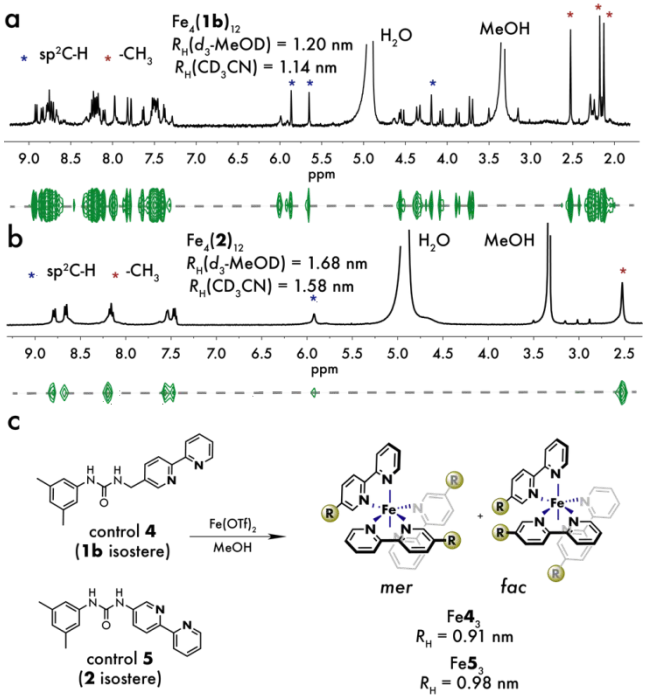

titration experiments by gradually increasing the polarity of the media with addition of DMSO or water into an acetonitrile solution of S_4-Fe$_4$(**1b**)$_{12}$, T-Fe$_4$**2**$_{12}$ and S_4-Fe$_4$**3**$_{12}$. As shown in Figure 5a, the cage S_4-Fe$_4$(**1b**)$_{12}$ is exceptionally stable; traces of the cage were still detected in solvent mixtures containing up to 31% (v/v) d_6-DMSO and 64% D_2O (v/v). Full H to D exchange of N-H protons was achieved at ca. 16% (v/v) content of D_2O. Cage T-Fe$_4$**2**$_{12}$ displays similar stability, surviving in as much as 22% (v/v) d_6-DMSO in CD_3CN (Fig. 5c). The addition of D_2O resulted in full H to D exchange at ca.

Figure 6. ^{1}H NMR spectra and DOSY trace of S_4-Fe$_4$(**1b**)$_{12}$ (a) and T-Fe$_4$**2**$_{12}$ (b) in d_3-MeOD; (c) Chemical structures and hydrodynamic radii of control compounds **4** and **5**.

14% D_2O and caused only slight shift of resonances assigned to aromatic and vinylic protons. Cage S_4-Fe$_4$**3**$_{12}$ was detected at d_6-DMSO and D_2O contents of up to 52% and 29%, respectively.

In the case of S_4-Fe$_4$(**1b**)$_{12}$ and T-Fe$_4$**2**$_{12}$, the H/D exchange rate of N-H protons with D_2O correlates with their pK_a values and inversely with the strength of the H-bonds they form. In both cases, the least acidic N-H proton **c** exchanged at the slowest rate. Surprisingly, these protons exchanged even slower than the N-H protons **a**, involved in intramolecular H-bonding. This observation cannot be explained by solvent accessibility alone since all N-H protons of the UPy$_2$ dimer in complex T-Fe$_4$**2**$_{12}$ are residing on the surface, and thus are equally accessible to D_2O. Contrarily, in cage S_4-Fe$_4$**3**$_{12}$, one full set of protons exchanged slower suggesting either markedly different stability of one particular pair of quadruple H-bonds or their reduced solvent accessibility (Fig. 5f).

Intrigued by the remarkable stability of these aggregates in polar solvents, we then characterized them in pure d_4-MeOD. In contrast to water, methanol provided sufficient solubility of complexes S_4-Fe$_4$(**1b**)$_{12}$ and T-Fe$_4$**2**$_{12}$ for ^{1}H NMR experiments (Fig. 6a-b).

The evaluation of the size of the complexes was made by using DOSY together with control ligands **4** and **5** containing a Bipy unit and non-H-bonding 1,3-dimethyl benzene isostere as the isocytosine ring (Fig. 6c). These controls can form only monomeric octahedron complexes Fe(**4**-**5**)$_3^{2+}$ and thus provided a reliable reference for the size of a single vertex of the tetrahedral assembly. The data obtained shows the formation of S_4-Fe$_4$(**1b**)$_{12}$ in d_3-MeOD based on both DOSY (single species), ^{1}H NMR (three sets of resonances) and ESI-MS experiments. DOSY measurements also indicate the formation of single species in the case of T-Fe$_4$**2**$_{12}$. Compared to diffusion coefficients obtained for controls Fe**4**$_3^{2+}$ and Fe**5**$_3^{2+}$, the so formed aggregates are much larger, in agreement with the formation of cage complexes. Moreover, the hydrodynamic radii of cage complexes are very close to the ones obtained in a CD_3CN solution. Unfortunately, the low solubility of the complex S_4-Fe$_4$**3**$_{12}$ in d_3-MeOD impeded the analogous experiments; however, the titration of a CD_3CN solution of the latter with an excess of d_3-MeOD also confirms the formation of the tetrahedron complex (Fig. S65, S104).

The stability of H-bonds in UPy$_2$ dimers in complexes S_4-Fe$_4$(**1b**)$_{12}$, T-Fe$_4$**2**$_{12}$ and S_4-Fe$_4$**3**$_{12}$ is exceptional and exceeds greatly the stability of cyclic tetrameric aggregates based on UPy aggregation, previously reported by us.[14e]

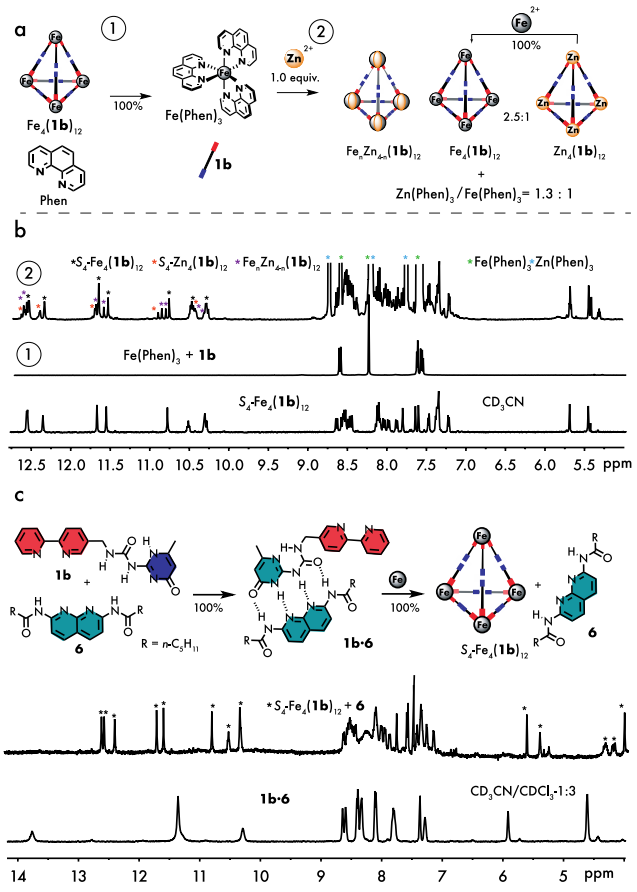

Figure 7. (a) Scheme depicting the disassembly of cage S_4-Fe$_4$(**1b**)$_{12}$ upon addition of phenanthroline (reaction 1) and the establishment of equilibrium of various species after introducing Zn^{2+} ions (reaction 2). Conversion of cage S_4-Zn$_4$(**1b**)$_{12}$ into cage S_4-Fe$_4$(**1b**)$_{12}$ is also indicated. (b) The ^{1}H NMR spectra are shown for reactions 1 and 2; (c) Formation of heterocomplex **1b-6** and its transformation to cage S_4-Fe$_4$(**1b**)$_{12}$ upon addition of Fe^{2+} ions.

To further evaluate the robustness of the complexes, we next performed experiments with external competitors for metal ion and H-bonds. First, a stoichiometric amount of phenanthroline (Phen) was added to the CD_3CN solution of S_4-Fe$_4$(**1b**)$_{12}$ (Fig. 7a, reaction 1). Owing to much stronger complexing properties of Phen compared to Bipy, the cage was fully converted into homoleptic Fe(Phen)$_3^{2+}$ and the free ligand **1b**. Addition of an equimolar amount of Zn(OTf)$_2$ to the above mixture resulted in a complex mixture with an unexpected speciation of species (Fig. 7a,b reaction 2). Instead of simple scavenging of the liberated **1b** by Zn^{2+} ions, the redistribution of metal ions between various species took place. In an equilibrated mixture, Zn(Phen)$_3^{2+}$ and Fe(Phen)$_3^{2+}$ were found in the molar ratio ~1.26, together with homoleptic cages S_4-Fe$_4$(**1b**)$_{12}$/S_4-Zn$_4$(**1b**)$_{12}$ (~2.5:1) and mixed cages Fe$_n$Zn$_{4-n}$(**1b**)$_{12}$ (Fig. S66-S67).[20] Independently, we also showed that cage S_4-Fe$_4$(**1b**)$_{12}$ is much more stable than S_4-Zn$_4$(**1b**)$_{12}$ (Fig. 7a, Fig. S71). Interestingly, the distribution of Fe^{2+} and Zn^{2+} within M(Phen)$_3^{2+}$ (M = metal) complexes favors otherwise less stable Zn(Phen)$_3^{2+}$. Based on lgK_3 values, the Fe(Phen)$_3^{2+}$ is more stable than Zn(Phen)$_3^{2+}$ by four orders of magnitude,[21] and the control experiment with Fe(Phen)$_3^{2+}$ and added Zn(OTf)$_2$ shows that Fe(Phen)$_3^{2+}$ remains in the mixture as the dominant species together with concomitant formation of Zn(Phen)$^{2+}$ and Zn(Phen)$_2^{2+}$, and no Zn(Phen)$_3^{2+}$ (Fig. S70). Moreover, the same species as in reaction 2 are also formed in the control experiment in which equimolar amounts of S_4-Fe$_4$(**1b**)$_{12}$ and S_4-Zn$_4$(**1b**)$_{12}$ were mixed, thus ruling out the presence of mixed species of the type M$_n$(**1b**)$_m$(Phen)$_l$ (M = metal) (Fig. S68). These results show that the combination of Fe/Zn/Phen and Fe/Zn/**1b** subsets, where the resulting equilibrium manifold becomes overwhelmed by the equilibrium between cage complexes resulting in the formation of S_4-Fe$_4$(**1b**)$_{12}$ as the dominant complex. Surprisingly, the metal exchange between cages is very fast, observed shortly after mixing the components.[22,23] The importance of the formation of cage complexes to the outcome of species distribution was also corroborated by another control experiment. Namely, repeating the same experiment (reactions 1 and 2) and replacing the cage forming ligand **1b** with simple Bipy, the homoleptic complexes Fe(Phen)$_3^{2+}$ and Zn(Bipy)$_3^{2+}$ were found to be the major products, whereas scrambled complexes formed only to a small extent (Fig. S72). The driving force for metal scrambling within cages is most likely of both enthalpic and entropic origin. Borrowing Fe^{2+} from S_4-Fe$_4$(**1b**)$_{12}$ to form the mixed cage Fe$_n$Zn$_{4-n}$(**1b**)$_{12}$ results in an increase of cage stability compared to S_4-Zn$_4$(**1b**)$_{12}$, at the same time preserving a large concentration of the most stable species, S_4-Fe$_4$(**1b**)$_{12}$, and increasing the entropy of the system. The example described herein thus provides a simple system from which a complicated reaction network can be built that is relevant to systems chemistry.

The stability of UPy$_2$ dimer within cage S_4-Fe$_4$(**1b**)$_{12}$ was also probed by using the powerful competing agent for ADDA H-bonding array - 2,7-diamido-1,8-naphthyridine (DAN) (Fig. 7c).[24] DAN is a non-self-complementary H-bonding motif that is only weakly aggregating in solution. On the other hand, it forms a very stable ADDA-DAAD heterocomplex with UPy (K_a = 10^7 M^{-1} in $CDCl_3$), and even though the value of K_a is comparable to those of the UPy dimerization (enol and keto forms), the heterocomplex is favored because of the increase of the total number of H-bonds in the system. Even highly stable cyclic supramolecular constructs assembled using cooperative UPy dimerization is fully disintegrated by the action of DAN.[14e]

In our hands, treating the complex S_4-Fe$_4$(**1b**)$_{12}$ with an excess of DAN derivative **6** resulted in no changes in ^{1}H NMR spectrum. Moreover, the pre-formed heterodimer **1b-6** is also transformed into cage S_4-Fe$_4$(**1b**)$_{12}$ and free DAN upon addition of Fe(OTf)$_2$, indicating the remarkable stability of the H-bonds of the UPy$_2$ dimers in S_4-Fe$_4$(**1b**)$_{12}$. In fact, to our knowledge this is the first example of UPy$_2$ dimers that resists DAN. This can be explained by the cooperative action of the network of coordination and H-bonds within the cage structure.

Finally, the assembly and disassembly of S_4-Fe$_4$(**1b**)$_{12}$ can also be controlled by the action of acid and base. The cage was fully destroyed by adding an excess of trifluoroacetic acid, and then regenerated to some extent by neutralizing with triethylamine (Fig. S74).

Self-sorting studies: effect of ligand structure. Having complexes S_4-Fe$_4$(**1**)$_{12}$, T-Fe$_4$**2**$_{12}$ and S_4-Fe$_4$**3**$_{12}$ in hand we became interested in whether the length or rigidity of the ligands can have any influence on the fidelity of the assembly process. The precise control of the assembly process within a mixture with multiple species present is one of the main goals of systems chemistry towards creation of adaptive molecular networks.[12,25]

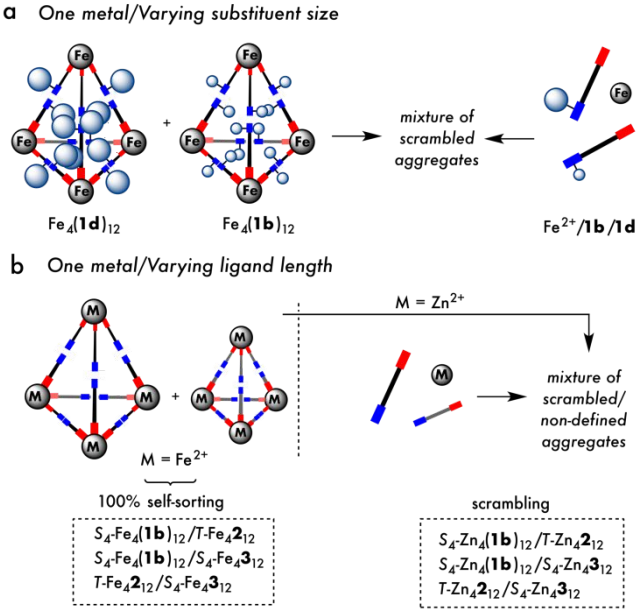

Figure 8. Self-sorting of molecular cages composed of the same type of ligands **1b** and **1d** having substituents of different size (a) and self-sorting of preformed cages having different types of ligands (b).

As shown in the previous mixing experiments (Fig.7a), two cages of the same type built from two different metals of similar size (Fe^{2+}/Zn^{2+}) resulted in scrambling of the metal ions to produce a significant amount of mixed-metal cages. We next probed the possibility for self-sorting based on the variation of the ligand. First, two 1st generation ligands **1b** and **1d** having CH_3- and $C_{11}H_{23}$- substituents in the isocytosine ring were

mixed together in 1:1 ratio followed by addition of a stoichiometric amount of $Fe(OTf)_2$. The formation of a complex mixture with no dominant species was noted (Fig. 8a). To avoid kinetic trapping of intermediates along the assembly pathway, a control experiment was performed with separately prepared individual cages S_4-Fe_4(**1b**)$_{12}$ and S_4-Fe_4(**1d**)$_{12}$. Exchange of the ligands was observed shortly after mixing, resulting in the same complex spectral pattern (Fig. S75). DOSY experiments showed that all equilibrating species are of similar size and therefore represent isomeric cage complexes (Fig. S76). The mixing process is most likely driven by the increase of the entropy, and also by the release of steric crowding in S_4-Fe_4(**1d**)$_{12}$. Unfortunately, it was not possible to prove whether the mixing process involved exchange of free ligands (or their dimers) *via* monomer dissociation or exchange of intact vertices *via* selective H-bond cleavage. Self-sorting experiments with pairs of preformed complexes Fe_4(**1b**)$_{12}$/Fe_4**2**$_{12}$, Fe_4(**1b**)$_{12}$/Fe_4**3**$_{12}$ and Fe_4**2**$_{12}$/Fe_4**3**$_{12}$ comprised of different ligands revealed full narcissistic self-sorting even after sonicating the solution at 50ºC overnight (Fig. 8b). Mixing of the free ligands with $Fe(OTf)_2$, however, resulted in a kinetically trapped state consisting of various aggregates (Fig. S80-S81). In stark contrast, the more labile Zn cages afforded a mixture of scrambled aggregates even at room temperature reaching equilibrium after 15 minutes (Fig. 8b, Fig. S82-S84).

Influence of the radius of metal ion. So far, using Fe^{2+} ($r_{(2+)}$ = 61 pm) or Zn^{2+} ($r_{(2+)}$ = 74 pm) ions as metal nodes resulted in formation of tetrahedral cages as the sole products. We next posed the question whether larger metal ions would provide enough space for UPy_2 to deliver different molecular architectures such as helicates or cubic cages. For this purpose, we decided to explore Hg^{2+} as a suitable candidate having one of the largest ionic radii ($r_{(2+)}$ = 116 pm) among the transition metals. Surprisingly, supramolecular chemistry of homoleptic mercury complexes HgL_3^{2+} with Bipy or Phen ligands is almost unexplored and only few examples of $Hg(Bipy)_3^{2+}$ or $Hg(Phen)_3^{2+}$ have been reported.[26] These complexes can only be obtained from mercury salts with weakly coordinating counterions, such as triflates, perchlorates or hexafluorosilicates; otherwise, formation of complexes $Hg(Phen/Bipy)_{n=1,2}X_2$ (X = halogen, rodanide, etc.) is preferred as a result of the soft character of Hg^{2+} and the hard nature of the Phen/Bipy ligands.[27] Because of the lack of ligand field stabilization energy ($5d^{10}$ electronic configuration) in their coordination compounds, there is no particular coordination geometry preferred by Hg^{2+} ions. Intrigued by the possible outcome, we prepared the corresponding complex by mixing **1b** and $Hg(OTf)_2$ in 3:1 ratio in CD_3CN. The ^{1}H NMR spectrum indicated the formation of the complex by displaying one set of rather broadened resonances (Fig. 9b). ESI-MS data supported the binuclear species, *i.e.* complexes Hg_2(**1b**)$_6$ (Fig. 9a, Fig. S86). To our delight, the presence of heavy atoms allowed us to unambiguously confirm its structure by using X-ray diffraction of the crystals grown by using vapor diffusion of chloroform into an acetonitrile solution. The data revealed the unprecedented molecular structure of the helicate (Fig. 9c, Page S57). Namely, three UPy_2 dimers in their keto tautomeric form are perfectly π-π stacked along the helicate axis with distance between aromatic planes of isocytosines d = 3.4 Å. The π-π stacking of the UPy_2 dimers provides an energetically favorable way to avoid steric clash between them, however, this requires larger separation of the Bipy units at the metal nodes. For this reason, the helicate of this type is obtained only with the large Hg^{2+} ions, and not with Fe^{2+}. The broad N-H resonances in the ^{1}H NMR might result from the overlap of the resonances of three non-equivalent UPy_2 dimers having similar chemical shifts. Another possibility is the fast (on the NMR timescale) interconversion of H-bonding networks between three π-π stacked dimers giving rise to averaged signals.

The comparison of the relative stabilities of Hg_2(**1b**)$_6$ and S_4-Fe_4(**1b**)$_{12}$ was made by adding a stoichiometric amount of $Fe(OTf)_2$ into the solution of the helicate. Formation of S_4-Fe_4(**1b**)$_{12}$ was noted together with new species having one set of resonances (Fig. 9b). The latter was shown by ESI-MS and independent synthesis to be rod-shaped Hg_2(**1b**)$_2(OTf)_4$ (Fig. S107-S108). Surprisingly, the equilibrium was not affected even in the presence of a large excess of Fe^{2+}. The exceptionally stable Hg_2(**1b**)$_2(OTf)_4$ might thus be useful in more complicated systems chemistry setups providing a reservoir for ligand **1b** other than Fe^{2+} or by building heterometallic architectures.

Modulation of self-assembly by H-bonding molecular inserts. The H-bonded nature of the edges in the cages described herein render them amenable for structural modifications and stimuli-responsiveness using external H-bonding molecular blocks that have a high affinity for UPy. As discussed above (Fig. 7c), the addition of DAN to ligand **1b** indeed provided the corresponding heterodimer in quantitative yield. Although mono-DAN derivative **6** (Fig. 7c) is readily expelled from the heterodimer in the presence of Fe^{2+}, we speculated that the bis-DAN derivative could be in principle inserted into the tetrahedron edge leading to either a change in topology or dimensions of the aggregate. For the proof-of-principle, bis-DAN insert **7** containing a flexible adipic acid linker was synthesized. The attempt to insert **7** directly into preformed cage S_4-Fe_4(**1b**)$_{12}$ in CD_3CN, however, was not successful (Fig. 10a, reaction 2). Mixing **1b**, **7** and $Fe(OTf)_2$ components together gave the same result, most likely due to solubility issues (Fig. 10a, reaction 1). Compound **7** is completely insoluble in acetonitrile, whereas

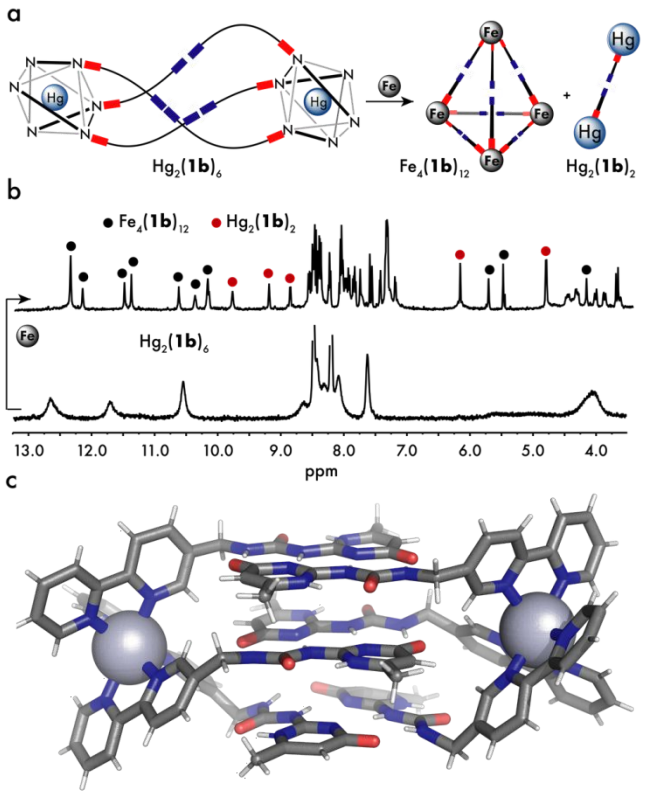

Figure 9. (a) Schematic representation of helicate $Hg_2(\mathbf{1b})_6$ and its conversion to cage S_4-$Fe_4(\mathbf{1b})_{12}$ and $Hg_2(\mathbf{1b})_2(OTf)_4$ upon addition of Fe^{2+} ions; (b) ^1H NMR spectra of $Hg_2(\mathbf{1b})_6$ and the reaction mixture shown in (a); (c) X-ray structure of helicate $Hg_2(\mathbf{1b})_6$.

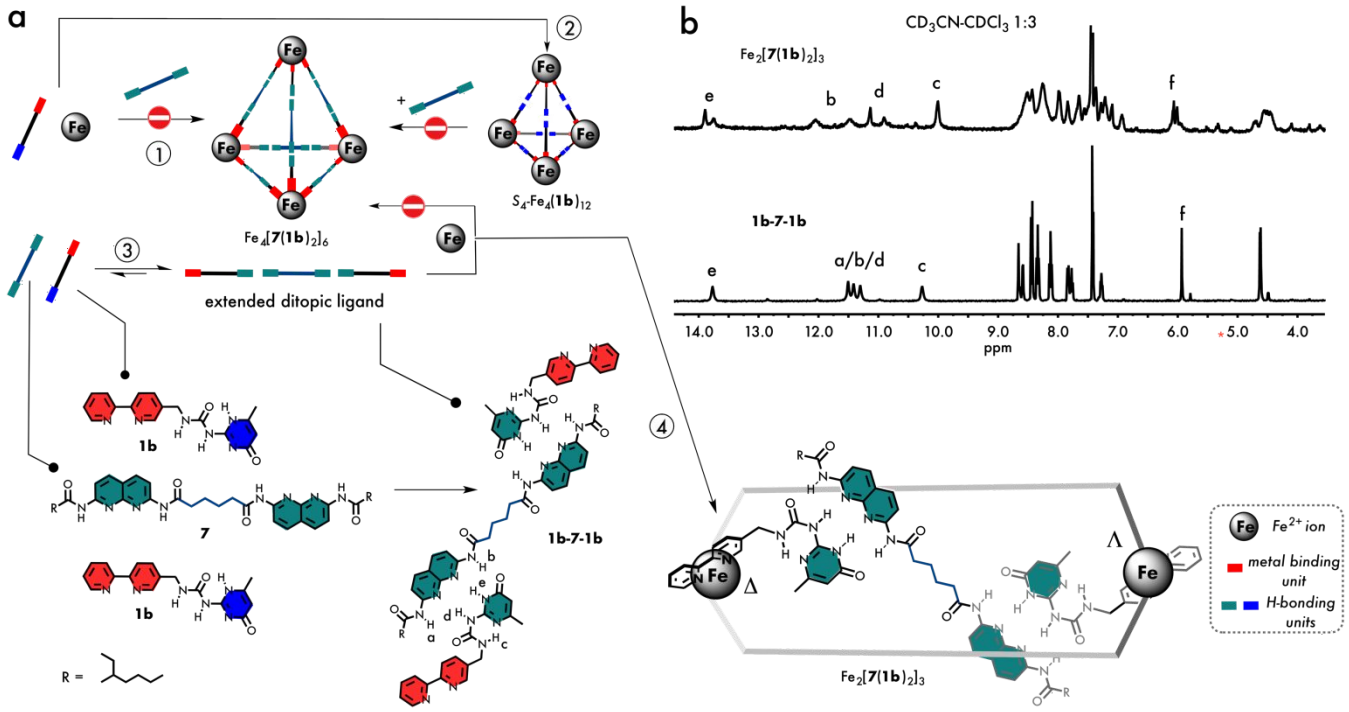

Figure 10. (a) Reaction 1: unsuccessful attempt to produce an extended cage $Fe_4[\mathbf{7}(\mathbf{1b})_2]_6$ using three component reaction between Fe^{2+}, **1b** and **7**. Reaction 2: unsuccessful attempt to insert bis-DAN derivative **7** into preformed cage S_4-$Fe_4(\mathbf{1b})_{12}$. Reaction 3: formation of heterocomplex **1b-7-1b**. Reaction 4: reaction of **1b-7-1b** with Fe^{2+} to produce mesocate $Fe_2[\mathbf{7}(\mathbf{1b})_2]_3$; (b) ^1H NMR spectra of heterocomplex **1b-7-1b** (bottom) and mesocate $Fe_2[\mathbf{7}(\mathbf{1b})_2]_3$ (top).

the also poorly soluble **1b** is gradually and selectively brought into solution during complexation. Hence, the formation of heterocomplex **1b-7-1b** is not possible. Finally, after switching to a mixed solvent CD_3CN:$CDCl_3$-1:3 system, the 1:2 mixture of **7** and **1b** afforded a clean ^1H NMR spectrum assigned to heterocomplex **1b-7-1b** (Fig. 10a, reaction 3). After addition of $Fe(OTf)_2$, a new spectrum consisting of a set of 10 resonances was obtained (Fig. 10b). The resonances corresponding to two protons at 12.07 ppm, 11.46 ppm and 9.99 ppm were not fully resolved due to similar values of chemical shifts. The spectrum is thus suggestive of two non-equivalent UPy-DAN heterodimers within the assembly. ESI-MS analysis indicated the formation of dinuclear species $Fe_2[\mathbf{7}(\mathbf{1b})_2]_3$, and not the extended cage $Fe_4[\mathbf{7}(\mathbf{1b})_2]_6$ (Fig. S109). The obtained results can be rationalized by assuming the formation of a triple-stranded structure with opposite Δ and Λ chirality at each six-coordinated metal center, *i.e.* a mesocate.[28] Based on the fact that the most stable conformation for alkyl chain is a zigzag, Albrecht *et al.* has proposed that a carbon chain linker comprised of an even number would favour a helicate, while a chain with an odd number of carbon atoms would result in a mesocate.[29] Our results contradict this rule. In fact, Raymond *et al.* and others[30,9b] have shown that formulating any general selection rule might be impossible due to stabilization of one of the aggregates by the formation of a host-guest complex with solvent molecules or counter anions. We assume that the selectivity towards a mesocate observed in our case stems from the bulkiness of the UPy-DAN unit. The formation of a helicate aggregate using S-shaped conformation of **1b-7-1b** would result in steric clash between UPy-DAN heterodimers, which on the other hand can be relieved in a mesocate formed from the pseudo-C conformation of **1b-7-1b**, as argued previously by Wu.[9b]

Host-guest chemistry. Tetrahedron cages are well documented to display rich host-guest chemistry having implications to catalysis, separation, or modulation of chemical reactivity of the complexed chemical entities.[2] To demonstrate the encapsulat

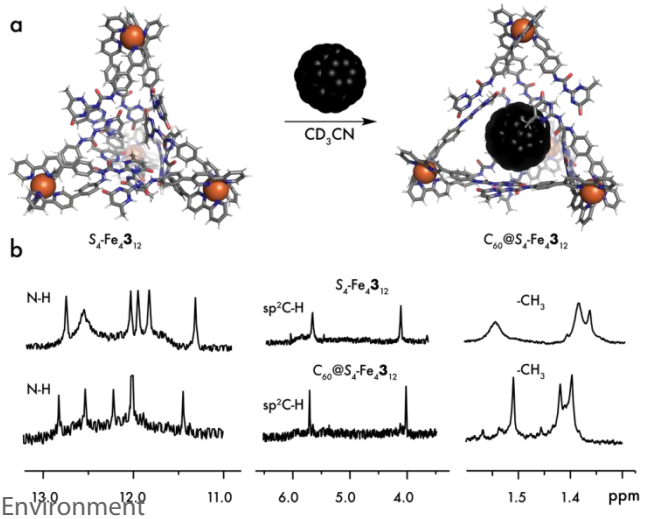

Figure 11. Molecular model of host-guest complex C_{60}@ S_4-Fe_4**3**$_{12}$ (a) and ^{1}H NMR spectra of cage S_4-Fe_4**3**$_{12}$ (top) and C_{60}@ S_4-Fe_4**3**$_{12}$ (bottom) (b).

ion ability of the hybrid cages described herein, we have chosen S_4-Fe_4**3**$_{12}$ as a model system because of its largest metal-metal distance. Fullerene C_{60} was selected as representative guest due to its high symmetry, its importance to material science and growing interest in the application of supramolecular cages for site selective functionalization.[31] Although the calculated cavity in S_4-Fe_4**3**$_{12}$ is too small for encapsulation of C_{60}, molecular modelling studies suggested that S_4-Fe_4**3**$_{12}$ can accommodate C_{60} after rotation of the C_{Ar}-N_{urea} bond without a change in the overall symmetry. Heating the mixture of an excess of C_{60} and S_4-Fe_4**3**$_{12}$ in CD_3CN resulted in the formation of the corresponding inclusion complex C_{60}@S_4-Fe_4**3**$_{12}$, which was of the same symmetry as the free host based on ^{1}H NMR results (Fig. 11). Full conversion to the inclusion complex was confirmed by a control experiment using only 0.5 equivalent of C_{60}. The spectrum consisted of two sets of resonances corresponding to free and complexed host in slow equilibrium (Fig. S89-S90). Similar diffusion coefficients were found for both species indicating that the host undergoes no significant structural changes upon complexation. The ESI-MS spectrum shows the ions derived from C_{60}@S_4-Fe_4**3**$_{12}$, and no signals of the cubic Fe_8**3**$_{24}$ or C_{60}@Fe_8**3**$_{24}$ impurities were detected. Although we were not able to accurately determine the association constant K_a using UV-vis spectroscopy, the lower limit of $K_a \geq 10^6$ M^{-1} can be estimated from ^{1}H NMR experiments (see Page S61).

The results obtained highlight the potential of this type of cages in various applications relying on the host-guest chemistry.

CONCLUSIONS

In conclusion, we have demonstrated the fully diastereoselective assembly of supramolecular tetrahedral cages by using the cooperative action of coordination and quadruple H-bonds. The dynamic H-bonds embedded into the edges of a tetrahedron scaffold open up new ways for structural and functional modulation of these assemblies and might also facilitate the ingress of relevant species into the cavity. In addition, the enhanced stability of H-bonds allowed the formation of tetrahedral complexes even in highly competitive protic media which renders them prospective cavitands for non-polar or anion (in)organic guests. We have realized for the first time the selection of a mesocate over a tetrahedral cage motif by modifying the rigidity of the ligand via insertion of flexible non-covalent wedge. The use of the large Hg^{2+} ion provided yet another approach to direct the assembly process towards dinuclear triple-stranded architectures. The Fe^{2+} tetrahedron cages obtained from ligands of different lengths showed no ligand scrambling when mixed together. These findings pave the way for simultaneous use of several cages for host-guest applications or synthetic cascades. Moreover, the possibility to exchange metal ions within the cage was demonstrated. The herein introduced molecular tetrahedron cages are potentially useful as receptors for guests as large as C_{60}. Further studies aiming to employ the host-guest chemistry of these cages in catalysis are undergoing.

ASSOCIATED CONTENT

Supporting Information

Experimental procedures and spectroscopic data (PDF)
X-ray diffraction data files (cif)

The Supporting Information is available free of charge on the ACS Publications website.

AUTHOR INFORMATION

Corresponding Author

* ias_qxshi@njtech.edu.cn

Notes

The authors declare no competing financial interest.

ACKNOWLEDGMENT

Q. S. acknowledges the financial support from the Natural Science Foundation of Jiangsu Province (BK20181375), Nanjing Tech University (Start-up Grant 39837129) and the State Key Laboratory of Fine Chemicals (KF1707). Q. S. is indebted to SICAM Fellowship from Jiangsu National Synergetic Innovation Center for Advanced Materials for financial support. A. N. acknowledges the PhD scholarship from Research Council of Lithuania. The authors thank Dr Rong Zhang for the initial attempt of HRMS.

REFERENCES

1. (a) Stang, P. J.; Olenyuk, B. Self-Assembly, Symmetry, and Molecular Architecture: Coordination as the Motif in the Rational Design of Supramolecular Metallacyclic Polygons and Polyhedra. *Acc. Chem. Res*. **1997**, *30*, 502-518. (b) Chakrabarty, R.; Mukherjee, P. S.; Stang, P. J. Supramolecular Coordination: Self-Assembly of Finite Two- and Three-Dimensional Ensembles. *Chem. Rev.* **2011**, *111*, 6810-6918. (c) Cook, T. R.; Stang, P. J. Recent Developments in the Preparation and Chemistry of Metallacycles and Metallacages via Coordination. *Chem. Rev*. **2015**, *115*, 7001-7045. (d) Fujita, M.; Tominaga, M.; Hori, A.; Therrien, B. Coordination Assemblies from a Pd(II)-Cornered Square Complex. *Acc. Chem. Res*. **2005**, *38*, 371-380. (e) Ward, M. D. Polynuclear Coordination Cages. *Chem. Commun*. **2009**, 4487-4499. (f) Smulders, M. M. J.; Riddell, I. A.; Browne, C.; Nitschke, J. R. Building on Architectural Principles for Three-Dimensional Metallosupramolecular Construction. *Chem. Soc. Rev*. **2013**, *42*, 1728-1754.

2. (a) Kusukawa, T.; Fujita, M. "Ship-in-a-Bottle" Formation of Stable Hydrophobic Dimers of *cis*-Azobenzene and -Stilbene Derivatives in a Self-Assembled Coordination Nanocage. *J. Am. Chem. Soc.* **1999**, *121*, 1397-1398. (b) Tashiro, S.; Tominaga, M.; Kawano, M.; Therrien, B.; Ozeki, T.; Fujita, M. Sequence-Selective Recognition of Peptides within the Single Binding Pocket of a Self-Assembled Coordination Cage. *J. Am. Chem. Soc.* **2005**, *127*, 4546-4547. (c) Ronson, T. K.; Meng, W.; Nitschke, J. R. Design Principles for the Optimization of Guest Binding in Aromatic Paneled $Fe^{II}_4L_6$ Cages. *J. Am. Chem. Soc.* **2017**, *139*, 9698-9707.

3. (a) Yoshizawa, M.; Klosterman, J. K.; Fujita, M. Functional Molecular Flasks: New Properties and Reactions within Discrete, Self-Assembled Hosts. *Angew. Chem. Int. Ed*. **2009**, *48*, 3418-3438. (b) Kaphan, D. M.; Toste, F. D.; Bergman, R. G.; Raymond, K. N. Enabling New Modes of Reactivity via Constrictive Binding in a Supramolecular-Assembly-Catalyzed Aza-Prins Cyclization. *J. Am. Chem. Soc.* **2015**, *137*, 9202-9205. (c) Yoshizawa, M.; Tamura, M.; Fujita, M. Diels-Alder in Aqueous Molecular Hosts: Unusual Regioselectivity and Efficient Catalysis. *Science* **2006**, *312*, 251-254. (d) Pluth, M. D.; Bergman, R. G.; Raymond, K. N. Proton-Mediated Chemistry and Catalysis in a Self-Assembled Supramolecular Host. *Acc. Chem. Res*. **2009**, *42*, 1650-1659. (e) Wang, Q.-Q.; Gonell, S.; Leenders, S. H. A. M.; Dürr, M.; Ivanović-Burmazović, I.; Reek, J. N.

H. Self-Assembled Nanospheres with Multiple Endohedral Binding Sites Pre-Organize Catalysts and Substrates for Highly Efficient Reactions. *Nat. Chem.* **2016**, *8*, 225-230.

4. (a) Mal, P.; Breiner, B.; Rissanen, K.; Nitschke, J. R. White Phosphorus is Air-Stable within a Self-Assembled Tetrahedral Capsule. *Science* **2009**, *324*, 1697-1699. (b) Yoshizawa, M.; Kusukawa, T.; Fujita, M.; Yamaguchi, K. Ship-in-a-Bottle Synthesis of Otherwise Labile Cyclic Trimers of Siloxanes in a Self-Assembled Coordination Cage. *J. Am. Chem. Soc.* **2000**, *122*, 6311-6312. (c) Yoshizawa, M.; Kusukawa, T.; Fujita, M.; Sakamoto, S.; Yamaguchi, K. Cavity-Directed Synthesis of Labile Silanol Oligomers within Self-Assembled Coordination Cages. *J. Am. Chem. Soc.* **2001**, *123*, 10454-10459.

5. (a) Suzuki, K.; Takao, K.; Sato, S.; Fujita, M. Coronene Nanophase within Coordination Spheres: Increased Solubility of C_{60}. *J. Am. Chem. Soc.* **2010**, *132*, 2544-2545. (b) Zhang, D.; Ronson, T. K.; Mosquera, J.; Martinez, A.; Nitschke, J. R. Selective Anion Extraction and Recovery Using a $Fe^{II}_4L_4$ Cage. *Angew. Chem. Int. Ed.* **2018**, *57*, 3717-3721. (c) Zhang, W.-Y.; Lin, Y.-J.; Han, Y.-F.; Jin, G.-X. Facile Separation of Regioisomeric Compounds by a Heteronuclear Organometallic Capsule. *J. Am. Chem. Soc.* **2016**, *138*, 10700-10707.

6. (a) Frischmann, P. D.; Kunz, V.; Würthner, F. Bright Fluorescence and Host–Guest Sensing with a Nanoscale M_4L_6 Tetrahedron Accessed by Self-Assembly of Zinc–Imine Chelate Vertices and Perylene Bisimide Edges. *Angew. Chem. Int. Ed*. **2015**, *54*, 7285-7289. (b) Neelakandan, P. P.; Jiménez, A.; Nitschke, J. R. Fluorophore Incorporation Allows Nanomolar Guest Sensing and White-Light Emission in M_4L_6 Cage Complexes. *Chem. Sci.* **2014**, *5*, 908-915. (c) Wang, M.; Vajpayee, V.; Shanmugaraju, S.; Zheng, Y.-R.; Zhao, Z.; Kim, H.; Mukherjee, P. S.; Chi, K.-W.; Stang, P. J. Coordination-Driven Self-Assembly of M_3L_2 Trigonal Cages from Preorganized Metalloligands Incorporating Octahedral Metal Centers and Fluorescent Detection of Nitroaromatics. *Inorg. Chem.* **2011**, *50*, 1506-1512.

7. Inokuma, Y.; Yoshioka, S.; Ariyoshi, J.; Arai, T.; Hitora, Y.; Takada, K.; Matsunaga, S.; Rissanen, K.; Fujita, M. X-Ray Analysis on the Nanogram to Microgram Scale Using Porous Complexes. *Nature* **2013**, *495*, 461-466.

8. (a) Li, X.-Z.; Zhou, L.-P.; Yan, L.-L.; Yuan, D.-Q.; Lin, C.-S.; Sun, Q.-F. Evolution of Luminescent Supramolecular Lanthanide $M_{2n}L_{3n}$ Complexes from Helicates and Tetrahedra to Cubes. *J. Am. Chem. Soc.* **2017**, *139*, 8237-8244. (b) Rizzuto, F. J.; Nitschke, J. R. Stereochemical Plasticity Modulates Cooperative Binding in a $Co^{II}_{12}L_6$ Cuboctahedron. *Nat. Chem*. **2017**, *9*, 903-908. (c) Roberts, D. A.; Pilgrim, B. S.; Sirvinskaite, G.; Ronson, T. K.; Nitschke, J. R. Covalent Post-Assembly Modification Triggers Multiple Structural Transformations of a Tetrazine-Edged Fe_4L_6 Tetrahedron. *J. Am. Chem. Soc*. **2018**, *140*, 9616-9623. (d) Caulder, D. L.; Brückner, C.; Powers, R. E.; König, S.; Parac, T. N.; Leary, J. A.; Raymond, K. N. Design, Formation and Properties of Tetrahedral M_4L_4 and M_4L_6 Supramolecular Clusters. *J. Am. Chem. Soc*. **2001**, *123*, 8923-8938.

9. (a) Scherer, M.; Caulder, D. L.; Johnson, D. W.; Raymond, K. N. Triple Helicate—Tetrahedral Cluster Interconversion Controlled by Host–Guest Interactions. *Angew. Chem. Int. Ed.* **1999**, *38*, 1587-1592. (b) Cui, F.; Li, S.; Jia, C.; Mathieson, J. S.; Cronin, L.; Yang, X.-J.; Wu, B. Anion-Dependent Formation of Helicates versus Mesocates of Triple-Stranded M_2L_3 ($M = Fe^{2+}$, Cu^{2+}) Complexes. *Inorg. Chem.* **2012**, *51*, 179-187.

10. For reviews, see: (a) Crassous, J. Chiral Transfer in Coordination Complexes: towards Molecular Materials. *Chem. Soc. Rev*. **2009**, *38*, 830-845. (b) Constable, E. C. Stereogenic Metal Centres – from Werner to Supramolecular Chemistry. *Chem. Soc. Rev*. **2013**, *42*, 1637-1651. (c) Chen, L.-J.; Yang, H.-B.; Shionoya, M. Chiral Metallosupramolecular Architectures. *Chem. Soc. Rev*. **2017**, *46*, 2555-2576. (d) Castilla, A. M.; Ramsay, W. J.; Nitschke, J. R. Stereochemistry in Subcomponent Self-Assembly. *Acc. Chem. Res.* **2014**, *47*, 2063-2073.

11. (a) Terpin, A. J.; Ziegler, M.; Johnson, D. W.; Raymond, K. N. Resolution and Kinetic Stability of a Chiral Supramolecular Assembly Made of Labile Components. *Angew. Chem. Int. Ed.* **2001**, *40*, 157-160. (b) Ousaka, N.; Clegg, J. K.; Nitschke, J. R. Nonlinear Enhancement of Chiroptical Response through Subcomponent Substitution in M_4L_6 Cages. *Angew. Chem. Int. Ed.* **2012**, *51*, 1464-1468. (c) Sun, B.; Nurttila, S. S.; Reek, J. N. H. Synthesis and Characterization of Self-Assembled Chiral $Fe^{II}_2L_3$ Cages. *Chem. Eur. J.* **2018**, *24*, 14693-14700. (d) Castilla, A. M.; Ousaka, N.; Bilbeisi, R. A.; Valeri, E.; Ronson, T. K.; Nitschke, J. R. High-Fidelity Stereochemical Memory in a $Fe^{II}_4L_4$ Tetrahedral Capsule. *J. Am. Chem. Soc.* **2013**, *135*, 17999-18006. (e) Castilla, A. M.; Miller, M. A.; Nitschke, J. R.; Smulders, M. M. J. Quantification of Stereochemical Communication in Metal–Organic Assemblies. *Angew. Chem. Int. Ed.* **2016**, *55*, 10616-10620. (f) Bell, Z. R.; Jeffery, J. C.; McCleverty, J. A.; Ward, M. D. Assembly of a Truncated-Tetrahedral Chiral $[M_{12}(\mu\text{-}L)_{18}]^{24+}$ Cage. *Angew. Chem. Int. Ed.* **2002**, *41*, 2515-2518. (g) Ye, Y.; Cook, T. R.; Wang, S.-P.; Wu, J.; Li, S.; Stang, P. J. Self-Assembly of Chiral Metallacycles and Metallacages from a Directionally Adaptable BINOL-Derived Donor. *J. Am. Chem. Soc.* **2015**, *137*, 11896-11899. (h) Bagdžiūnas, G.; Butkus, E.; Orentas, E. Hierarchical Assembly toward Nanoparticles of a Chiral Palladium Supramolecular Complex Based on Bicyclo[3.3.1]nonane Framework. *Organometallics* **2019**, *38*, 2647-2653. (i) Enemark, E. J.; Stack, T. D. P. Stereospecificity and Self-Selectivity in the Generation of a Chiral Molecular Tetrahedron by Metal-Assisted Self-Assembly. *Angew. Chem. Int. Ed.* **1998**, *37*, 932-935. (j) Imai, Y.; Yuasa, J. Supramolecular Chirality Transformation Driven by Monodentate Ligand Binding to a Coordinatively Unsaturated Self-Assembly Based on C_3-Symmetric Ligands. *Chem. Sci.* **2019**, *10*, 4236-4245.

12. (a) Salles, Jr., A. G.; Zarra, S.; Turner, R. M.; Nitschke, J. R. A Self-Organizing Chemical Assembly Line. *J. Am. Chem. Soc.* **2013**, *135,* 19143-19146. (b) Campbell, V. E.; de Hatten, X.; Delsuc, N.; Kauffmann, B.; Huc, I.; Nitschke, J. R. Cascading Transformations within a Dynamic Self-Assembled System. *Nat. Chem.* **2010**, *2*, 684-687. (c) Wood, C. S.; Browne, C.; Wood, D. M.; Nitschke, J. R. Fuel-Controlled Reassembly of Metal−Organic Architectures. *ACS Cent. Sci.* **2015**, *1*, 504-509.

13. (a) Zhang, D.; Ronson, T. K.; Nitschke, J. R. Functional Capsules via Subcomponent Self-Assembly. *Acc. Chem. Res.* **2018**, *51*, 2423-2436. (b) Ronson, T. K.; Zarra, S.; Black, S. P.; Nitschke, J. R. Metal–Organic Container Molecules through Subcomponent Self-Assembly. *Chem. Commun.* **2013**, *49*, 2476-2490.

14. Selected examples on the importance of tautomerism in defining self-assembly outcome: (a) Račkauskaitė, D.; Bergquist, K.-E.; Shi, Q.; Sundin, A.; Butkus, E.; Wärnmark, K.; Orentas, E. A Remarkably Complex Supramolecular Hydrogen-Bonded Decameric Capsule Formed from an Enantiopure C_2-Symmetric Monomer by Solvent-Responsive Aggregation. *J. Am. Chem. Soc.* **2015**, *137*, 10536-10546. (b) Shi, Q.; Javorskis, T.; Bergquist, K.-E.; Ulčinas, A.; Niaura, G.; Matulaitienė, I.; Orentas, E.; Wärnmark, K. Stimuli-Controlled Self-Assembly of Diverse Tubular Aggregates from one Single Small Monomer. *Nat. Commun.* **2017**, *8*, 14943. (c) Račkauskaitė, D.; Gegevičius, R.; Matsuo, Y.; Wärnmark, K.; Orentas, E. An Enantiopure Hydrogen-Bonded Octameric Tube: Self-Sorting and Guest-Induced Rearrangement. *Angew. Chem. Int. Ed.* **2016**, *55*, 208-212. (d) Neniškis, A.; Račkauskaitė, D.; Shi, Q.; Robertson, A. J.; Marsh, A.; Ulčinas, A.; Valiokas, R.; Brown, S. P.; Wärnmark, K.; Orentas, E. A Tautoleptic Approach to Chiral Hydrogen-Bonded Supramolecular Tubular Polymers with Large Cavity. *Chem. Eur. J.* **2018**, *24*, 14028-14033. (e) Shi, Q.; Bergquist, K.-E.; Huo, R.; Li, J.; Lund, M.; Vácha, R.; Sundin, A.; Butkus, E.; Orentas, E.; Wärnmark, K. Composition- and Size-Controlled Cyclic Self-Assembly by Solvent- and C_{60}-Responsive Self-Sorting. *J. Am. Chem. Soc.* **2013**, *135*, 15263-15268. (f) Chen, Q.; Su, X.; Orentas, E.; Shi, Q. Supramolecular Crowns: a New Class of Cyclic Hydrogen-Bonded Cavitands. *Org. Chem. Front*. **2019**, *6*, 611-617.

15. (a) Marshall, L. J.; de Mendoza, J. Self-Assembled Squares and Triangles by Simultaneous Hydrogen Bonding and Metal Coordination. *Org. Lett.* **2013**, *15*, 1548-1551. (b) Sommer, S. K.; Zakharov, L. N.; Pluth, M. D. Design, Synthesis, and Characterization of Hybrid Metal−Ligand Hydrogen-Bonded (MLHB) Supramolecular Architectures. *Inorg. Chem.* **2015**, *54*, 1912-1918. (c) Gianneschi, N. C.; Tiekink, E. R. T.; Rendina, L. M. Dinuclear Platinum Complexes with Hydrogen-Bonding Functionality: Noncovalent Assembly of Nanoscale Cyclic Arrays. *J. Am. Chem. Soc.* **2000**, *122*, 8474-8479. (d) Sigel, R. K. O.; Freisinger, E.; Metzger, S.; Lippert, B. Metalated

Nucleobase Quartets: Dimerization of a Metal-Modified Guanine, Cytosine Pair of *trans*-$(NH_3)_2Pt^{II}$ and Formation of CH···N Hydrogen Bonds. *J. Am. Chem. Soc.* **1998**, *120*, 12000-12007. (e) Appavoo, D.; Carnevale, D.; Deschenaux, R.; Therrien, B. Combining Coordination and Hydrogen-Bonds to Form Arene Ruthenium Metalla-Assemblies. *J. Organomet. Chem*. **2016**, *824*, 80-87.

16. For the simultaneous use of quadruple H-bonds and coordination bonds in supramolecular polymers, see: (a) Hofmeier, H.; Hoogenboom, R.; Wouters, M. E. L.; Schubert, U. S. High Molecular Weight Supramolecular Polymers Containing both Terpyridine Metal Complexes and Ureidopyrimidinone Quadruple Hydrogen-Bonding Units in the Main Chain. *J. Am. Chem. Soc*. **2005**, *127*, 2913-2921. (b) Yan, X.; Li, S.; Pollock, J. B.; Cook, T. R.; Chen, J.; Zhang, Y.; Ji, X.; Yu, Y.; Huang, F.; Stang, P. J. Supramolecular Polymers with Tunable Topologies via Hierarchical Coordination-Driven Self-Assembly and Hydrogen Bonding Interfaces *Proc. Natl. Acad. Sci. U.S.A.* **2013**, *110*, 15585-15590; (c) Yan, X.; Jiang, B.; Cook, T. R.; Zhang, Y.; Li, J.; Yu, Y.; Huang, F.; Yang, H.-B.; Stang, P. J. Dendronized Organoplatinum(II) Metallacyclic Polymers Constructed by Hierarchical Coordination-Driven Self-Assembly and Hydrogen-Bonding Interfaces. *J. Am. Chem. Soc.* **2013**, *135*, 16813-16816.

17. (a) Beijer, F. H.; Sijbesma, R. P.; Kooijman, H.; Spek, A. L.; Meijer, E. W. Strong Dimerization of Ureidopyrimidones via Quadruple Hydrogen Bonding. *J. Am. Chem. Soc*. **1998**, *120*, 6761-6769. (b) Sijbesma, R. P.; Beijer, F. H.; Brunsveld, L.; Folmer, B. J. B.; Hirschberg, J. H. K. K.; Lange, R. F. M.; Lowe, J. K. L.; Meijer, E. W. Reversible Polymers Formed from Self-Complementary Monomers Using Quadruple Hydrogen Bonding. *Science* **1997**, *278*, 1601-1604.

18. (a) Meng, W.; Clegg, J. K.; Thoburn, J. D.; Nitschke, J. R. Controlling the Transmission of Stereochemical Information through Space in Terphenyl-Edged Fe_4L_6 Cages. *J. Am. Chem. Soc*. **2011**, *133*, 13652-13660. (b) Ousaka, N.; Grunder, S.; Castilla, A. M.; Whalley, A. C.; Stoddart, J. F.; Nitschke, J. R. Efficient Long-Range Stereochemical Communication and Cooperative Effects in Self-Assembled Fe_4L_6 Cages. *J. Am. Chem. Soc*. **2012**, *134*, 15528-15537. (c) Meng, W.; Ronson, T. K.; Nitschke, J. R. Symmetry Breaking in Self-Assembled M_4L_6 Cage Complexes. *Proc. Natl. Acad. Sci. U.S.A*. **2013**, *110*, 10531-10535.

19. Giri, C.; Topić, F.; Mal, P.; Rissanen, K. Self-Assembly of a M_4L_6 Complex with Unexpected S_4 Symmetry. *Dalton Trans.* **2014**, *43*, 17889-17892.

20. ESI-MS spectrum indicated the presence of all mixed species $FeZn_3(\mathbf{1b})_{12}$, $Fe_2Zn_2(\mathbf{1b})_{12}$ and $Fe_3Zn(\mathbf{1b})_{12}$. On the other hand, the high intensity of resonances at 10.84 ppm and 10.89 ppm and their 1:1 ratio are indicative of the dominance of one particular species. The control experiments with different Fe^{2+}/Zn^{2+} ratio support this assumption. See Fig. S68.

21. (a) Makrlik, E.; Vaňura, P. Stability Constants of Tris(2,2′-bipyridine) Complexes of Fe^{2+}, Co^{2+}, Ni^{2+}, Cu^{2+} and Zn^{2+} in 1,2-Dichloroethane Saturated with Water. *Colloids Surf.* **1992**, *68*, 195-197. (b) Irving, H.; Mellor, D. H. The Stability of Metal Complexes of 1,10-Phenanthroline and its Analogues. Part I. 1,10-Phenanthroline and 2,2′-bipyridyl. *J. Chem. Soc*. **1962**, 5222-5237.

22. Cage complexes can show remarkable kinetic inertness even if they contain nominally labile metal centres, see: Sato, S.; Ishido, Y.; Fujita, M. Remarkable Stabilization of $M_{12}L_{24}$ Spherical Frameworks through the Cooperation of 48 Pd(II)-Pyridine Interactions. *J. Am. Chem. Soc.* **2009**, *131*, 6064-6065 and ref. 1e.

23. Hall, B. R.; Manck, L. E.; Tidmarsh, I. S.; Stephenson, A.; Taylor, B. F.; Blaikie, E. J.; Griend, D. A. V.; Ward, M. D. Structures, Host–Guest Chemistry and Mechanism of Stepwise Self-Assembly of M_4L_6 Tetrahedral Cage Complexes. *Dalton Trans*. **2011**, *40*, 12132-12145.

24. (a) Park, T.; Todd, E. M.; Nakashima, S.; Zimmerman, S. C. A Quadruply Hydrogen Bonded Heterocomplex Displaying High-Fidelity Recognition. *J. Am. Chem. Soc*. **2005**, *127*, 18133-18142. (b) Park, T.; Zimmerman, S. C.; Nakashima, S. A Highly Stable Quadruply Hydrogen-Bonded Heterocomplex Useful for Supramolecular Polymer Blends. *J. Am. Chem. Soc*. **2005**, *127*, 6520-6521. (c) Park, T.; Zimmerman, S. C. Interplay of Fidelity, Binding Strength, and Structure in Supramolecular Polymers. *J. Am. Chem. Soc*. **2006**, *128*, 14236-14237.

25. (a) Smulders, M. M. J.; Jiménez, A.; Nitschke, J. R. Integrative Self-Sorting Synthesis of a $Fe_8Pt_6L_{24}$ Cubic Cage. *Angew. Chem. Int. Ed.* **2012**, *51*, 6681-6685. (b) Holloway, L. R.; Bogie, P. M.; Hooley, R. J. Controlled Self-Sorting in Self-Assembled Cage Complexes. *Dalton Trans.* **2017**, *46*, 14719-14723. (c) Caulder, D. L.; Raymond, K. N. Supramolecular Self-Recognition and Self-Assembly in Gallium(III) Catecholamide Triple Helices. *Angew. Chem. Int. Ed*. **1997**, *36*, 1440-1442. (d) Bloch, W. M.; Clever, G. H. Integrative Self-Sorting of Coordination Cages Based on 'Naked' Metal Ions. *Chem. Commun.* **2017**, *53*, 8506-8516.

26. (a) Deacon, G. B.; Raston, C. L.; Tunaley, D.; White, A. H. Crystal Structure of Tris(1,10-phenanthroline)mercury (II) Trifluoromethanesulfonate. *Aust. J. Chem*. **1979**, *32*, 2195-2201. (b) Swiatkowski, M.; Kruszynski, R. Revealing the Structural Chemistry of the Group 12 Halide Coordination Compounds with 2,2'-Bipyridine and 1,10-Phenanthroline. *J. Coord. Chem*. **2017**, *70*, 642-675.

27. (a) Amani, V.; Alizadeh, R.; Alavije, H. S.; Heydari, S. F.; Abafat, M. Mononuclear Mercury(II) Complexes Containing Bipyridine Derivatives and Thiocyanate Ligands: Synthesis, Characterization, Crystal Structure Determination, and Luminescent Properties. *J. Mol. Struct.* **2017**, *1142*, 92-101. (b) Mahmoudi, G.; Rafiei, S.; Morsali, A.; Zhu, L. G. Syntheses and Characterization of Three Mercury(II) Complexes, $[Hg(phen)_2(SCN)_2]$, $[Hg(2,2'\text{-bipy})_2(SCN)_2]$ and $[Hg(phen)_2(NO_3)_2]$, Thermal and Fluorescence Studies. *J. Coord. Chem*. **2008**, *61*, 789-795.

28. To ensure sufficient solubility, unsymmetrically branched DAN derivative **7** was used in our study. The stereogenic center at branching carbon renders this compound chiral. As prepared, compound **7** is a mixture of (*S,S*), (*R,R*) and (*R/S*) stereoisomers and in principle, might influence the stereochemical outcome of the assembly of **7**-**1b**-**7**. However, in our related studies using **7** and chiral UPy derivatives, we never observed any impact of the chiral side chain, perhaps due to its peripheral location. The exact 1:1 relationship of all integrals in the spectrum of $Fe_2[\mathbf{7}(\mathbf{1b})_2]_3$ suggests that the chirality of the side chain plays no role for directing the self-assembly.

29. (a) Albrecht, M.; Kotila, S. Formation of a "*meso*-Helicate" by Self-Assembly of Three Bis(catecholate) Ligands and Two Titanium(IV) Ions. *Angew. Chem. Int. Ed.* **1995**, *34*, 2134-2137. (b) Albrecht, M. "Let's Twist Again"-Double-Stranded, Triple-Stranded, and Circular Helicates. *Chem. Rev*. **2001,** *101*, 3457-3498.

30. Xu, J.; Parac, T. N.; Raymond, K. N. *meso* Myths: What Drives Assembly of Helical versus *meso*-$[M_2L_3]$ Clusters? *Angew. Chem. Int. Ed.* **1999**, *38*, 2878-2882.

31. (a) Lu, Z.; Lavendomme, R.; Burghaus, O.; Nitschke, J. R. A Zn_4L_6 Capsule with Enhanced Catalytic C-C Bond Formation Activity upon C_{60} Binding. *Angew. Chem. Int. Ed.* **2019**, *58*, 9073-9077. (b) Brenner, W.; Ronson, T. K.; Nitschke, J. R. Separation and Selective Formation of Fullerene Adducts within an $M^{II}_8L_6$ Cage. *J. Am. Chem. Soc.* **2017**, *139*, 75-78. (c) García-Simón, C.; Costas, M.; Ribas, X. Metallosupramolecular Receptors for Fullerene Binding and Release. *Chem. Soc. Rev.* **2016**, *45*, 40-62. (d) García-Simón, C.; Monferrer, A.; Garcia-Borràs, M.; Imaz, I.; Maspoch, D.; Costas, M.; Ribas, X. Size-Selective Encapsulation of C_{60} and C_{60}-Derivatives within an Adaptable Naphthalene-Based Tetragonal Prismatic Supramolecular Nanocapsule. *Chem. Commun.* **2019**, *55*, 798-801. (e) Han, W. K.; Zhang, H. X.; Wang, Y.; Liu, W.; Yan, X.; Li, T.; Gu, Z.-G. Tetrahedral Metal-Organic Cages with Cube-Like Cavities for Selective Encapsulation of Fullerene Guests and Their Spin-Crossover Properties. *Chem. Commun.* **2018**, *54*, 12646-12649. (f) Martínez-Agramunt, V.; Eder, T.; Darmandeh, H.; Guisado-Barrios, G.; Peris, E. A Size-Flexible Organometallic Box for the Encapsulation of Fullerenes. *Angew. Chem. Int. Ed.* **2019**, *58*, 5682-5686. (g) Mahata, K.; Frischmann, P. D.; Würthner, F. Giant Electroactive M_4L_6 Tetrahedral Host Self-Assembled with Fe(II) Vertices and Perylene Bisimide Dye Edges. *J. Am. Chem. Soc.* **2013**, *135*, 15656-15661. (h) Fuertes-Espinosa, C.; García-Simón, C.; Castro, E.; Costas, M.; Echegoyen, L.; Ribas, X. A Copper-Based Supramolecular Nanocapsule that Enables Straightforward Purification of Sc_3N-Based Endohedral Metallofullerene Soots. *Chem. Eur. J.* **2017**, *23*, 3553-3557. (i) Fuertes-Espinosa, C.; Gómez-Torres, A.; Morales-Martínez, R.; Rodríguez-Fortea, A.; García-Simón, C.; Gándara, F.; Imaz, I.; Juanhuix, J.; Maspoch, D.; Poblet, J. M.; Echegoyen, L.; Ribas, X.

Purification of Uranium-Based Endohedral Metallofullerenes (EMFs) by Selective Supramolecular Encapsulation and Release. *Angew. Chem. Int. Ed.* **2018**, *57*, 11294-11299. (j) Colomban, C.; Szalóki, G.; Allain, M.; Gómez, L.; Goeb, S.; Sallé, M.; Costas, M.; Ribas, X. Reversible C_{60} Ejection from a Metallocage through the Redox-Dependent Binding of a Competitive Guest. *Chem. Eur. J.* **2017**, *23*, 3016-3022. (k) García-Simón, C.; Garcia-Borràs, M.; Gómez, L.; Parella, T.; Osuna, S.; Juanhuix, J.; Imaz, I.; Maspoch, D.; Costas, M.; Ribas, X. Sponge-Like Molecular Cage for Purification of Fullerenes. *Nat. Commun.* **2014**, *5,* 5557 (l) Sánchez-Molina, I.; Grimm, B.; Calderon, R. M. K.; Claessens, C. G.; Guldi, D. M.; Torres, T. Self-Assembly, Host-Guest Chemistry, and Photophysical Properties of Subphthalocyanine-Based Metallosupramolecular Capsules. *J. Am. Chem. Soc.* **2013**, *135*, 10503-10511. (m) Nakamura, T.; Ube, H.; Miyake, R.; Shionoya, M. A C_{60}-Templated Tetrameric Porphyrin Barrel Complex via Zinc-Mediated Self-Assembly Utilizing Labile Capping Ligands. *J. Am. Chem. Soc.* **2013**, *135*, 18790-18793.

TOC graphics